

The radiative efficiency of neutron stars at low-level accretion

Erlin Qiao^{1,2★} and B.F. Liu^{1,2}

¹Key Laboratory of Space Astronomy and Technology, National Astronomical Observatories, Chinese Academy of Sciences, Beijing 100101, China

²School of Astronomy and Space Sciences, University of Chinese Academy of Sciences, 19A Yuquan Road, Beijing 100049, China

Accepted XXX. Received YYY; in original form ZZZ

ABSTRACT

When neutrons star low-mass X-ray binaries (NS-LMXBs) are in the low-level accretion regime (i.e., $L_X \lesssim 10^{36}$ erg s⁻¹), the accretion flow in the inner region around the NS is expected to be existed in the form of the hot accretion flow, e.g., the advection-dominated accretion flow (ADAF) as that in black hole X-ray binaries. Following our previous studies in Qiao & Liu 2020a and 2020b on the ADAF accretion around NSs, in this paper, we investigate the radiative efficiency of NSs with an ADAF accretion in detail, showing that the radiative efficiency of NSs with an ADAF accretion is much lower than that of $\epsilon \sim \frac{MGM}{R_*} / Mc^2 \sim 0.2$ despite the existence of the hard surface. As a result, given a X-ray luminosity L_X (e.g., between 0.5 and 10 keV), \dot{M} calculated by $\dot{M} = L_X \frac{R_*}{GM}$ is lower than the real \dot{M} calculated within the framework of the ADAF accretion. The real \dot{M} can be more than two orders of magnitude higher than that of calculated by $\dot{M} = L_X \frac{R_*}{GM}$ with appropriate model parameters. Finally, we discuss that if applicable, the model of ADAF accretion around a NS can be applied to explain the observed millisecond X-ray pulsation in some NS-LMXBs (such as PSR J1023+0038, XSS J12270-4859 and IGR J17379-3747) at a lower X-ray luminosity of a few times of 10^{33} erg s⁻¹, since at this X-ray luminosity the calculated \dot{M} with the model of ADAF accretion can be high enough to drive a fraction of the matter in the accretion flow to be channelled onto the surface of the NS forming the X-ray pulsation.

Key words: accretion, accretion discs – stars: neutron – black hole physics – X-rays: binaries

1 INTRODUCTION

Currently, there are two types of accretion flow around compact objects [black holes (BH) and neutron stars (NS)], i.e., the geometrically thin, optically thick, cold accretion disc (Shakura & Sunyaev 1973), and the geometrically thick, optically thin, hot accretion flow, such as the advection-dominated accretion flow (ADAF) (Yuan & Narayan 2014, for review). The cold accretion disc with a higher mass accretion rate is widely used to explain the optical/UV emission in luminous active galactic nuclei (AGNs), and the X-ray emission of X-ray binaries at the high/soft state (e.g. Mitsuda et al. 1984; Makishima et al. 1986). While the ADAF with a lower mass accretion rate is often used to explain the dominant emission in low-luminosity AGNs, as well as the low/hard and the quiescent state of X-ray binaries (Done et al. 2007, for review).

In general, the cold accretion disc is a kind of radiatively efficient accretion flow in both BH case and NS case. In the approximation of the Newtonian mechanics, for a non-rotating BH, the radiative efficiency of the accretion disc is $\epsilon = \frac{1}{2} \frac{MGM}{3R_S} / Mc^2 \sim 0.1$ (with G being the gravitational constant, \dot{M} being the mass accretion rate in units of g s⁻¹, c being the speed of light, and R_S being the

Schwarzschild radius with $R_S = 2GM/c^2 \approx 2.95 \times 10^5 M/M_\odot$ cm), i.e., half of the gravitational energy will be released out in the form of the electromagnetic radiation in the accretion disc. While for a NS, the radiative efficiency of the accretion is $\epsilon = \frac{MGM}{R_*} / Mc^2 \sim 0.2$ (taking $M = 1.4M_\odot$, and $R_* = 12.5$ km¹), which is obtained as that half of the gravitational energy will be released out in the accretion disc and the other half of the gravitational energy will be released out in a thin boundary layer between the accretion disc and the surface of the NS in the form of the electromagnetic radiation (Gilfanov & Sunyaev 2014).

In general, the ADAF solution is a kind of radiatively inefficient accretion flow in BH case. In the approximation of the Newtonian mechanics, for a non-rotating BH, the radiative efficiency of the ADAF is $\epsilon < \frac{1}{2} \frac{MGM}{3R_S} / Mc^2 \sim 0.1$ (Ichimaru 1977; Rees et al. 1982; Narayan & Yi 1994, 1995; Manmoto et al. 1997; Yuan & Narayan 2014, for review). This is due to the optically thin nature of the ADAF solution, a fraction of the viscously dissipated energy in the ADAF is stored in the gas of the ADAF as the internal energy, and finally advected into the event horizon of the BH with-

¹ We take $R_* = 12.5$ because we intend to keep the same efficiency of the gravitational energy release between a NS and a non-rotating BH. If the NS mass $m = 1.4$ is taken, the corresponding NS radius is $R_* = 12.5$ km.

* E-mail: qiaoe@nao.cas.cn

out radiation. The fraction of the viscously dissipated energy stored in the gas of the ADAF as the internal energy is dependent on \dot{M} , and this fraction increases with decreasing \dot{M} , which means that the radiative efficiency of the ADAF around a BH decreases with decreasing \dot{M} . Specifically, when \dot{M} is close to the critical mass accretion rate \dot{M}_{crit} of the ADAF ($\dot{M}_{\text{crit}} \sim \alpha^2 \dot{M}_{\text{Edd}}$, with α being the viscosity parameter, and $\dot{M}_{\text{Edd}} = L_{\text{Edd}}/0.1c^2 \approx 1.39 \times 10^{18} M/M_{\odot} \text{ g s}^{-1}$ being the Eddington scaled mass accretion rate, where L_{Edd} is defined as $L_{\text{Edd}} = 1.26 \times 10^{38} M/M_{\odot} \text{ erg s}^{-1}$), the value of ϵ is close to 0.1 as that of the cold accretion disc around a BH (Xie & Yuan 2012). However, when \dot{M} is significantly less than \dot{M}_{crit} , the radiative efficiency ϵ decreases dramatically with decreasing \dot{M} , and the value of ϵ is much less than 0.1 (Xie & Yuan 2012, for discussions).

In this paper, we focus on the radiative efficiency of the ADAF solution around a NS (strictly speaking, it is the radiative efficiency of NSs with an ADAF accretion, since a fraction of the ADAF energy released at the surface of the NS can finally radiate out to be observed). The dynamics of the ADAF around a weakly magnetized NS has been investigated by some authors previously (Medvedev & Narayan 2001; Medvedev 2004; Narayan & Yi 1995). In general, one of the most difficult problems for the study of the ADAF around a NS is how to treat the dynamics and radiation of the boundary layer between the surface of the NS and the ADAF. The physics of the boundary layer can significantly affect the global dynamics and radiation of the ADAF (Medvedev & Narayan 2001; Medvedev 2004; D'Angelo et al. 2015). Recently, in a series of papers, i.e., Qiao & Liu (2018), Qiao & Liu (2020a), and Qiao & Liu (2020b), we study the dynamics and the radiation of the ADAF around a weakly magnetized NS in the framework of the self-similar solution of the ADAF by simplifying the physics of the boundary layer. Specifically, we introduce a parameter, f_{th} , which describes the fraction of the ADAF energy released at the surface of the NS as thermal emission to be scattered in the ADAF. Under this assumption, i.e., considering the radiative feedback between the surface of the NS and the ADAF, we self-consistently calculate the structure and the corresponding emergent spectrum of the NS with an ADAF accretion. The value of f_{th} can affect the radiative efficiency of NSs with an ADAF accretion. Physically, the value of f_{th} is uncertain. However, it has been shown that the value of f_{th} can be constrained in a relatively narrow range by comparing with the observed X-ray spectra (typically between 0.5 and 10 keV) of neutron star low-mass X-ray binaries (NS-LMXBs), since the value of f_{th} can affect both the shape and the luminosity of the X-ray spectra (Qiao & Liu 2020a,b). The results in Qiao & Liu (2020a,b) jointly suggest that the value of f_{th} is certainly less than 0.1, and a smaller value of $f_{\text{th}} \sim 0.01$ is more preferred.

In this paper, following the results of Qiao & Liu (2020a,b) for the constraints to the value of f_{th} , we investigate the radiative efficiency of NSs with an ADAF accretion for taking two typical values of f_{th} as that of $f_{\text{th}} = 0.1$, and $f_{\text{th}} = 0.01$ respectively. The radiative efficiency is defined as $\epsilon_{\text{bol}} = L_{\text{bol}}/\dot{M}c^2$ (with L_{bol} being the bolometric luminosity). Based on the emergent spectra of NSs with an ADAF accretion for the bolometric luminosity, we find that ϵ_{bol} is nearly a constant with \dot{M} for either taking $f_{\text{th}} = 0.1$ or taking $f_{\text{th}} = 0.01$. The value of ϵ_{bol} for $f_{\text{th}} = 0.1$ is roughly one order of magnitude lower than the previously expected value of $\epsilon \sim \frac{MG\dot{M}}{R_*}/\dot{M}c^2 \sim 0.2$, and ϵ_{bol} for $f_{\text{th}} = 0.01$ is roughly two orders of magnitude lower than the value of $\epsilon \sim 0.2$. Then, we suggest that NSs with an ADAF accretion is radiatively inefficient despite the existence of the hard surface. Further, we investigate the radiative efficiency in some specific bands, e.g., $\epsilon_{0.5-10\text{keV}}$ and $\epsilon_{0.5-100\text{keV}}$ (defined as $\epsilon_{0.5-10\text{keV}} = L_{0.5-10\text{keV}}/\dot{M}c^2$

and $\epsilon_{0.5-100\text{keV}} = L_{0.5-100\text{keV}}/\dot{M}c^2$). $\epsilon_{0.5-10\text{keV}}$ is nearly same with $\epsilon_{0.5-100\text{keV}}$ for a fixed \dot{M} with $f_{\text{th}} = 0.1$ and $f_{\text{th}} = 0.01$ respectively. $\epsilon_{0.5-10\text{keV}}$ (or $\epsilon_{0.5-100\text{keV}}$) is less than ϵ_{bol} , so is certainly less than $\epsilon \sim \frac{MG\dot{M}}{R_*}/\dot{M}c^2 \sim 0.2$. Meanwhile, $\epsilon_{0.5-10\text{keV}}$ (or $\epsilon_{0.5-100\text{keV}}$) decreases very quickly with decreasing \dot{M} . As a result, for a NS-LMXB, if we intend to use the observed X-ray luminosity (e.g., between 0.5 and 10 keV) as the indicator for \dot{M} , \dot{M} calculated with the formula of $\dot{M} = L_X \frac{R_*}{GM}$ is lower than that of calculated with our model of ADAF accretion around a NS. Obviously, given a X-ray luminosity, the difference between the \dot{M} calculated with our model of ADAF accretion and the \dot{M} calculated with the formula of $\dot{M} = L_X \frac{R_*}{GM}$ depends on f_{th} , with the difference of the calculated \dot{M} increases with decreasing f_{th} .

Finally, in this paper, we argue that if applicable, the model of ADAF accretion around a NS can probably be used to explain the observed millisecond X-ray pulsation in some NS-LMXBs (such as PSR J1023+0038, XSS J12270-4859 and IGR J17379-3747) at a X-ray luminosity (between 0.5 and 10 keV) of a few times of $10^{33} \text{ erg s}^{-1}$, since at this X-ray luminosity the calculated \dot{M} with the model of ADAF accretion can be high enough, e.g., more than two orders of magnitude higher than that of calculated with the formula of $\dot{M} = L_X \frac{R_*}{GM}$ for taking $f_{\text{th}} = 0.01$, to drive a fraction of the matter in the accretion flow to be channelled onto the surface of the NS forming the X-ray pulsation. A brief summary on the ADAF model around a NS and the constraints to the value of f_{th} in Qiao & Liu (2020a,b) are introduced in Section 2. The results are shown in Section 3. The discussions are in Section 4 and the conclusions are in Section 5.

2 A SUMMARY ON QIAO & LIU 2020A,B

The structure and the corresponding emergent spectra of the ADAF around a NS are strictly investigated within the framework of the self-similar solution of the ADAF (Qiao & Liu 2018). In Qiao & Liu (2020a,b), we update the code with the effect of the NS spin considered compared with that of in Qiao & Liu (2018). In our model, there are seven parameters, i.e., the NS mass m ($m = M/M_{\odot}$), NS radius R_* , NS spin frequency ν_{NS} , mass accretion rate \dot{m} ($\dot{m} = \dot{M}/\dot{M}_{\text{Edd}}$), as well as the viscosity parameter α , and the magnetic parameter β [with magnetic pressure $p_m = B^2/8\pi = (1 - \beta)p_{\text{tot}}$, $p_{\text{tot}} = p_{\text{gas}} + p_m$] for describing the microphysics of the ADAF. The last parameter is, f_{th} , describing the fraction of the ADAF energy released at the surface of the NS as thermal emission to be scattered in the ADAF to cool the ADAF itself, which consequently controls the feedback between the ADAF and the NS. We always take $m = 1.4$, and R_* in the range of 10-12.5 km (Degenaar & Suleimanov 2018) [$R_* = 12.5$ km in Qiao & Liu (2020a), and $R_* = 10$ km in Qiao & Liu (2020b)]. In general, it has been proven that the effect of the NS spin frequency ν_{NS} on the structure and the emergent spectra of the ADAF around a NS is very little, and nearly can be neglected [see Figure 8 of Qiao & Liu (2020a) for taking $\nu_{\text{NS}} = 0, 200, 500, 700$ Hz respectively]. So we fix $\nu_{\text{NS}} = 0$ Hz in Qiao & Liu (2020a,b). The magnetic field in ADAF is very weak as suggested by the magnetohydrodynamic simulations (Yuan & Narayan 2014, for review). We fix $\beta = 0.95$ in Qiao & Liu (2020a,b).

The X-ray spectra of NS-LMXBs in the low-level accretion regime ($L_{0.5-10\text{keV}} \lesssim 10^{36} \text{ erg s}^{-1}$) can be described by a single power-law model, or a two-component model, i.e., a thermal soft X-ray component plus a power-law component. In general, if the *Swift* X-ray data are used, the spectral fitting with a sin-

gle power-law model can return an accepted fit. And if the high-quality *XMM – Newton* X-ray data are used, the spectra fitting with a two-component model can significantly improve the fitting results in some X-ray luminosity range, e.g., in the range of $L_{0.5-10\text{keV}} \sim 10^{34} - 10^{35} \text{ erg s}^{-1}$ (e.g. [Wijnands et al. 2015](#)). In [Qiao & Liu \(2020a\)](#), we test the effect of α and f_{th} on the X-ray spectra between 0.5 and 10 keV, and explain the fractional contribution of the power-law component η ($\eta \equiv L_{0.5-10\text{keV}}^{\text{power law}}/L_{0.5-10\text{keV}}$) (with the spectra fitted with the two-component model) as a function of the $L_{0.5-10\text{keV}}$ for a sample of non-pulsating NS-LMXBs in a wide range from $L_{0.5-10\text{keV}} \sim 10^{32} - 10^{36} \text{ erg s}^{-1}$. Observationally, there is a positive correlation between η and $L_{0.5-10\text{keV}}$ for $L_{0.5-10\text{keV}} \gtrsim$ a few times of $10^{33} \text{ erg s}^{-1}$, and an anticorrelation between η and $L_{0.5-10\text{keV}}$ for $L_{0.5-10\text{keV}} \lesssim$ a few times of $10^{33} \text{ erg s}^{-1}$. By comparing with the observed correlation (both the positive correlation and the anticorrelation) between η and $L_{0.5-10\text{keV}}$, it is found that the effect of α on the correlation between η and $L_{0.5-10\text{keV}}$ is very little, and nearly can be neglected. Meanwhile, it is found that the correlation between η and $L_{0.5-10\text{keV}}$ can be well matched by adjusting the value of f_{th} . The value of f_{th} is constrained to be less than 0.1. Especially, $f_{\text{th}} = 0.01$ is more preferred [see Figure 7 of [Qiao & Liu \(2020a\)](#)].

Further, in [Qiao & Liu \(2020b\)](#), based on the sample of non-pulsating NS-LMXBs in [Wijnands et al. \(2015\)](#), and adding some more non-pulsating NS-LMXBs from [Parikh et al. \(2017\)](#) and [Beri et al. \(2019\)](#), we explain the anticorrelation between the X-ray photon index Γ (obtained by fitting the X-ray spectra between 0.5 and 10 keV with a single power law) and $L_{0.5-10\text{keV}}$, i.e., the softening of the X-ray spectra with decreasing $L_{0.5-10\text{keV}}$, in the range of $L_{0.5-10\text{keV}} \sim 10^{34} - 10^{36} \text{ erg s}^{-1}$ by adjusting the value of f_{th} . Moreover, it is shown that a fraction of the sources in [Qiao & Liu \(2020b\)](#) are once reported to be fitted with the two-component model (with *XMM – Newton* X-ray data), i.e., a thermal soft X-ray component plus a power-law component. Combining the explanations for the anticorrelation between the X-ray photon index Γ and $L_{0.5-10\text{keV}}$ with the X-ray spectra analyzed with the single power-law model, and the positive correlation between η and $L_{0.5-10\text{keV}}$ with the two-component model for a fraction of the sources in the sample, we conclude that in the range of $L_{0.5-10\text{keV}} \sim 10^{34} - 10^{35} \text{ erg s}^{-1}$, the softening of the X-ray spectra is due to the increase of the thermal soft X-ray component, while in the range of $L_{0.5-10\text{keV}} \sim 10^{35} - 10^{36} \text{ erg s}^{-1}$, the softening of the X-ray spectra is probably due to the evolution of the power-law component itself. As a summary, in the study above for explaining the anticorrelation between Γ and $L_{0.5-10\text{keV}}$, it has been shown that the value of f_{th} can be constrained to be less than 0.1, and is very probably to be much smaller values, i.e., $\sim 0.003 - 0.005$ ([Qiao & Liu 2020b](#)).

In the following, fixing $m = 1.4$, $R_* = 12.5 \text{ km}$, $\nu_{\text{NS}} = 500 \text{ Hz}$ (see Section 3.2 for discussions), $\alpha = 0.3$ and $\beta = 0.95$, we investigate the radiative efficiency of NSs with an ADAF accretion for different \dot{m} by taking two typical values of f_{th} , i.e., $f_{\text{th}} = 0.1$ and $f_{\text{th}} = 0.01$ respectively.

3 RESULTS

3.1 Numerical results

We plot the emergent spectra of NSs with an ADAF accretion for different \dot{m} with $f_{\text{th}} = 0.1$ in panel (1) of Fig. 1, and with $f_{\text{th}} = 0.01$ in panel (2) of Fig. 1. Based on the emergent spectra in panel (1) of Fig. 1, we calculate three quantities, i.e., the X-ray luminosity

between 0.5 and 10 keV $L_{0.5-10\text{keV}}$, the X-ray luminosity between 0.5 and 100 keV $L_{0.5-100\text{keV}}$, and the bolometric luminosity L_{bol} for different \dot{m} with $f_{\text{th}} = 0.1$. Based on the emergent spectra in panel (2) of Fig. 1, a similar calculation is done for $L_{0.5-10\text{keV}}$, $L_{0.5-100\text{keV}}$, and L_{bol} for different \dot{m} with $f_{\text{th}} = 0.01$. In panel (1) of Fig. 2, we plot $L_{0.5-10\text{keV}}$, $L_{0.5-100\text{keV}}$, and L_{bol} as a function of \dot{m} for $f = 0.1$ and $f = 0.01$ respectively. Specifically, for $f = 0.1$, it can be seen that, all the three quantities $L_{0.5-10\text{keV}}$, $L_{0.5-100\text{keV}}$, and L_{bol} decrease with decreasing \dot{m} . Meanwhile, it can be seen that, for $f = 0.1$, $L_{0.5-10\text{keV}}$ as a function of \dot{m} is nearly overlapped with $L_{0.5-100\text{keV}}$ as a function of \dot{m} . This is because all the X-ray spectra are very soft for different \dot{m} with $f_{\text{th}} = 0.1$, the value of $L_{0.5-10\text{keV}}$ and $L_{0.5-100\text{keV}}$ is nearly same for a fixed \dot{m} . It also easy to see that, for $f = 0.1$, the value of L_{bol} is always greater than $L_{0.5-10\text{keV}}$ (or $L_{0.5-100\text{keV}}$). Meanwhile, the separation between L_{bol} and $L_{0.5-10\text{keV}}$ (or $L_{0.5-100\text{keV}}$) becomes larger and larger with decreasing \dot{m} . In general, the trends of $L_{0.5-10\text{keV}}$, $L_{0.5-100\text{keV}}$, and L_{bol} as a function of \dot{m} for $f = 0.01$ are similar to that of for $f = 0.1$ respectively. However, the values of $L_{0.5-10\text{keV}}$, $L_{0.5-100\text{keV}}$, and L_{bol} for $f = 0.01$ are systematically lower than that of for $f = 0.1$ for roughly one order of magnitude or more for a fixed \dot{m} respectively. We further plot the formula $L = \frac{MGM}{R_*}$ (note: $\dot{M} = \dot{m}\dot{M}_{\text{Edd}}$, $M = mM_{\odot}$) as a comparison, one can refer to the dashed line in panel (1) of Fig. 2 for clarity. It can be seen that all the three luminosities, i.e., $L_{0.5-10\text{keV}}$, $L_{0.5-100\text{keV}}$ and L_{bol} , are lower than the luminosity calculated with the formula of $L = \frac{MGM}{R_*}$ for a fixed \dot{M} (or \dot{m}).

We define three quantities for the radiative efficiency in different bands, i.e.,

$$\epsilon_{0.5-10\text{keV}} = L_{0.5-10\text{keV}}/\dot{M}c^2, \quad (1)$$

$$\epsilon_{0.5-100\text{keV}} = L_{0.5-100\text{keV}}/\dot{M}c^2, \quad (2)$$

$$\epsilon_{\text{bol}} = L_{\text{bol}}/\dot{M}c^2. \quad (3)$$

In panel (2) of Fig. 2, we plot $\epsilon_{0.5-10\text{keV}}$, $\epsilon_{0.5-100\text{keV}}$ and ϵ_{bol} as a function of \dot{m} with $f = 0.1$, and $f = 0.01$ respectively. Specifically, for $f_{\text{th}} = 0.1$, ϵ_{bol} is nearly a constant for different \dot{m} with $\epsilon_{\text{bol}} \sim 0.02$. $\epsilon_{0.5-10\text{keV}}$ as a function of \dot{m} is nearly overlapped with $\epsilon_{0.5-100\text{keV}}$ as a function of \dot{m} . For $f_{\text{th}} = 0.1$, $\epsilon_{0.5-10\text{keV}}$ decreases from ~ 0.013 to $\sim 1.6 \times 10^{-4}$ for \dot{m} decreasing from 1.1×10^{-2} to 1.0×10^{-5} , and $\epsilon_{0.5-100\text{keV}}$ decreases from ~ 0.016 to $\sim 1.6 \times 10^{-4}$ for \dot{m} decreasing from 1.1×10^{-2} to 1.0×10^{-5} . In general, the trends of $\epsilon_{0.5-10\text{keV}}$, $\epsilon_{0.5-100\text{keV}}$ and ϵ_{bol} as a function of \dot{m} for $f_{\text{th}} = 0.01$ are similar to that of for $f_{\text{th}} = 0.1$. For $f_{\text{th}} = 0.01$, ϵ_{bol} is also nearly a constant, decreasing slightly with decreasing \dot{m} , i.e., ϵ_{bol} decreasing from ~ 0.006 to ~ 0.002 for \dot{m} decreasing from 1.5×10^{-2} to 5.0×10^{-5} . For $f_{\text{th}} = 0.01$, $\epsilon_{0.5-10\text{keV}}$ as a function of \dot{m} is also nearly overlapped with $\epsilon_{0.5-100\text{keV}}$ as a function of \dot{m} . Specifically, $\epsilon_{0.5-10\text{keV}}$ decreases from ~ 0.002 to $\sim 2.2 \times 10^{-5}$ for \dot{m} decreasing from 1.5×10^{-2} to 5.0×10^{-5} . $\epsilon_{0.5-100\text{keV}}$ decreases from ~ 0.004 to $\sim 2.4 \times 10^{-5}$ for \dot{m} decreasing from 1.5×10^{-2} to 5.0×10^{-5} . Also as a comparison, we plot the radiative efficiency ϵ calculated with the formula of $\epsilon \sim \frac{MGM}{R_*}/\dot{M}c^2$, see the dashed line in panel (2) of Fig. 2. The value of ϵ is ~ 0.2 , which is roughly one order of magnitude higher than ϵ_{bol} for $f = 0.1$ and two orders of magnitude higher than ϵ_{bol} for $f = 0.01$.

In summary, based on our study above for taking $f_{\text{th}} = 0.1$ and $f_{\text{th}} = 0.01$, the predicted luminosity, i.e., $L_{0.5-10\text{keV}}$, $L_{0.5-100\text{keV}}$ and L_{bol} from our model of ADAF accretion, are all lower than the luminosity predicted by the formula of $L = \frac{MGM}{R_*}$ for a fixed \dot{M} (or \dot{m}). This in turn means that, given a value of $L_{0.5-10\text{keV}}$,

$L_{0.5-10\text{keV}}$ or L_{bol} , the obtained \dot{M} (or \dot{m}) from our model of ADAF accretion is greater than that of calculated with the formula of $\dot{M} = L \frac{R_*}{GM}$ (L can be $L_{0.5-10\text{keV}}$, $L_{0.5-100\text{keV}}$ or L_{bol}). Here we just take two X-ray luminosities between 0.5 and 10 keV, i.e., $L_{0.5-10\text{keV}} = 3.0 \times 10^{33}$ erg s $^{-1}$ and $L_{0.5-10\text{keV}} = 5.0 \times 10^{33}$ erg s $^{-1}$ as examples for calculating \dot{M} . One can refer to Fig. 3 for the illustrations and Table 1 for the detailed numerical results. Specifically, for $L_{0.5-10\text{keV}} = 3.0 \times 10^{33}$ erg s $^{-1}$, the mass accretion rate \dot{M}_0 calculated with the formula of $\dot{M}_0 = L_{0.5-10\text{keV}} \frac{R_*}{GM}$ is 2.02×10^{13} g s $^{-1}$, which is ~ 27 times less than the mass accretion rate $\dot{M}_{0.1}$ calculated with our model of ADAF accretion for taking $f_{\text{th}} = 0.1$, and is ~ 192 times less than the mass accretion rate $\dot{M}_{0.01}$ calculated with our model of ADAF accretion for taking $f_{\text{th}} = 0.01$. For $L_{0.5-10\text{keV}} = 5.0 \times 10^{33}$ erg s $^{-1}$, \dot{M}_0 calculated with the formula of $\dot{M}_0 = L_{0.5-10\text{keV}} \frac{R_*}{GM}$ is 3.36×10^{13} g s $^{-1}$, which is ~ 23 times less than $\dot{M}_{0.1}$ calculated with our model of ADAF accretion for taking $f_{\text{th}} = 0.1$, and is ~ 183 times less than $\dot{M}_{0.01}$ calculated with our model of ADAF accretion for taking $f_{\text{th}} = 0.01$. The relatively higher \dot{M} calculated from our model of ADAF accretion has very clear physical meanings, as will be discussed in Section 3.2.

3.2 Possible applications for explaining the formation of the millisecond X-ray pulsation at the X-ray luminosity of a few times of 10^{33} erg s $^{-1}$

Recently, the millisecond X-ray pulsations have been observed in several NS X-ray sources, such as, the transitional millisecond pulsar (tMSP) PSR J1023+0038 (Archibald et al. 2015) and XSS J12270-4859 (Papitto et al. 2015) as they are in the accretion-powered LMXB state, as well as the X-ray transient IGR J17379-3747 (Bult et al. 2019), at a lower X-ray luminosity (between 0.5 and 10 keV) of a few times of 10^{33} erg s $^{-1}$. This challenges the traditional accretion disc theory for the formation of the X-ray pulsation at such a low X-ray luminosity, since in general at this low X-ray luminosity (if the mass accretion rate calculated with formula of $\dot{M} = L_X \frac{R_*}{GM}$), the corotation radius of the NS accreting system is less than the magnetospheric radius. In this case, the ‘propeller’ effect may work, expelling (a fraction of) the matter in the accretion flow to be leaving away from the NS (Illarionov & Sunyaev 1975). In this paper, we suggest that, if applicable, our model of ADAF accretion may be applied to explain the observed millisecond X-ray pulsation at the X-ray luminosity of a few times of 10^{33} erg s $^{-1}$. This is because at this X-ray luminosity, \dot{M} calculated from our model of ADAF accretion for taking an appropriate value of f_{th} , such as $f_{\text{th}} = 0.01$, can be more than two orders of magnitude higher than that of calculated with the formula of $\dot{M} = L_X \frac{R_*}{GM}$ to make the magnetospheric radius less than the corotation radius. In this case, as the accretion flow moves inward, if the radius is less than the magnetospheric radius, (a fraction of) the matter in the accretion flow will be magnetically channelled onto the surface of the NS, leading to the formation of the X-ray pulsation.

For clarity, we list the expression of the corotation radius R_c and the magnetospheric radius R_m respectively as follows. The corotation radius R_c is expressed as,

$$R_c = \left(\frac{GM}{4\pi^2 \nu_{\text{NS}}^2} \right)^{1/3}$$

² We take these two X-ray luminosities since the X-ray pulsations have been confirmed in some NS-LMXBs in these luminosities, as will be discussed in Section 3.2.

$$\approx 26.6 \text{ km} \left(\frac{M}{1.4M_{\odot}} \right)^{1/3} \left(\frac{\nu_{\text{NS}}}{500 \text{ Hz}} \right)^{-2/3}, \quad (4)$$

where M is the NS mass, and ν_{NS} is the NS spin frequency. The magnetospheric radius R_m is expressed as (Sruitt & Taam 1993; D’Angelo & Sruitt 2010; D’Angelo et al. 2015),

$$\begin{aligned} R_m &= \left(\frac{\eta \mu^2}{4\Omega_{\text{NS}} \dot{M}} \right)^{1/5} \\ &\approx 24 \text{ km} \eta^{1/5} \left(\frac{B_*}{10^8 \text{ G}} \right)^{2/5} \left(\frac{R_*}{10 \text{ km}} \right)^{6/5} \\ &\quad \times \left(\frac{\nu_{\text{NS}}}{500 \text{ Hz}} \right)^{-1/5} \left(\frac{\dot{M}}{10^{16} \text{ g s}^{-1}} \right)^{-1/5}, \end{aligned} \quad (5)$$

where $\mu = B_* R_*^3$ is magnetic dipole moment (with B_* being the magnetic field at the surface of the NS, R_* being the NS radius), Ω_{NS} is the rotational angular velocity of the NS (with $\Omega_{\text{NS}} = 2\pi\nu_{\text{NS}}$), $\eta \leq 1$ is the dimensionless parameter describing the strength of the toroidal magnetic field induced by the relative rotation between the accretion flow and dipolar magnetic field, and \dot{M} is the mass accretion rate in units of g s $^{-1}$. We investigate the relation between R_c and R_m for PSR J1023+0038, XSS J12270-4859 and IGR J17379-3747 respectively as follows.

PSR J1023+0038: the millisecond X-ray pulsation of PSR J1023+0038 has been discovered at the X-ray luminosity of $L_{0.5-10\text{keV}} \sim 3.0 \times 10^{33}$ erg s $^{-1}$. The spin frequency of PSR J1023+0038 is $\nu_{\text{NS}} = 592$ Hz (Archibald et al. 2015). As we can see from Table 1, at the X-ray luminosity of $L_{0.5-10\text{keV}} \sim 3.0 \times 10^{33}$ erg s $^{-1}$, the mass accretion rate \dot{M}_0 calculated with the formula of $\dot{M}_0 = L_{0.5-10\text{keV}} \frac{R_*}{GM}$ is 2.02×10^{13} g s $^{-1}$. At this X-ray luminosity, the mass accretion rate $\dot{M}_{0.1}$ calculated with our model of ADAF accretion for $f_{\text{th}} = 0.1$ is 5.48×10^{14} g s $^{-1}$, and mass accretion rate $\dot{M}_{0.01}$ calculated with our model of ADAF accretion for $f_{\text{th}} = 0.01$ is 3.88×10^{15} g s $^{-1}$. If we assume $M = 1.4M_{\odot}$, $R_* = 12.5$ km as we take in Section 3.1 of this paper, a typical value of the magnetic field at the surface of the NS $B_* = 10^8$ G and $\eta = 0.1$, according to equation (4), $R_c \approx 23.8$ km, and according to equation (5), $R_{m0} \approx 66.2$ km, $R_{m0.1} \approx 34.2$ km, and $R_{m0.01} \approx 23.1$ km (with R_{m0} , $R_{m0.1}$ and $R_{m0.01}$ being the magnetospheric radii calculated by taking the mass accretion rate as \dot{M}_0 , $\dot{M}_{0.1}$ and $\dot{M}_{0.01}$ respectively). It can be seen that, if the mass accretion rate, i.e. \dot{M}_0 , is calculated with the formula of $\dot{M}_0 = L_{0.5-10\text{keV}} \frac{R_*}{GM}$, $R_{m0} > R_c$, theoretically, in this case the pulsation cannot be formed. If the mass accretion rate, i.e. $\dot{M}_{0.1}$, is calculated with our model of ADAF accretion for $f_{\text{th}} = 0.1$, $R_{m0.1} > R_c$, theoretically, the pulsation also cannot be formed. While, if the mass accretion rate, i.e. $\dot{M}_{0.01}$, is calculated with our model of ADAF accretion for $f_{\text{th}} = 0.01$, $R_{m0.01} < R_c$, theoretically, the pulsation can be formed (Illarionov & Sunyaev 1975).

XSS J12270-4859 and IGR J17379-3747: the millisecond X-ray pulsation of both XSS J12270-4859 and IGR J17379-3747 are discovered at the X-ray luminosity of $L_{0.5-10\text{keV}} \sim 5.0 \times 10^{33}$ erg s $^{-1}$. The spin frequency of XSS J12270-4859 and IGR J17379-3747 are $\nu_{\text{NS}} = 593$ Hz and $\nu_{\text{NS}} = 468$ Hz respectively. As we can see from Table 1, at the X-ray luminosity of $L_{0.5-10\text{keV}} = 5.0 \times 10^{33}$ erg s $^{-1}$, the mass accretion rate \dot{M}_0 calculated with the formula of $\dot{M}_0 = L_{0.5-10\text{keV}} \frac{R_*}{GM}$ is 3.36×10^{13} g s $^{-1}$. At this X-ray luminosity, the mass accretion rate $\dot{M}_{0.1}$ calculated with our model of ADAF accretion for $f_{\text{th}} = 0.1$ is 7.75×10^{14} g s $^{-1}$, and the mass accretion rate $\dot{M}_{0.01}$ calculated with our model of ADAF accretion for $f_{\text{th}} = 0.01$ is 6.15×10^{15} g s $^{-1}$. Also, if we assume $M = 1.4M_{\odot}$, $R_* = 12.5$ km, $B_* = 10^8$ G and $\eta = 0.1$ for both XSS J12270-

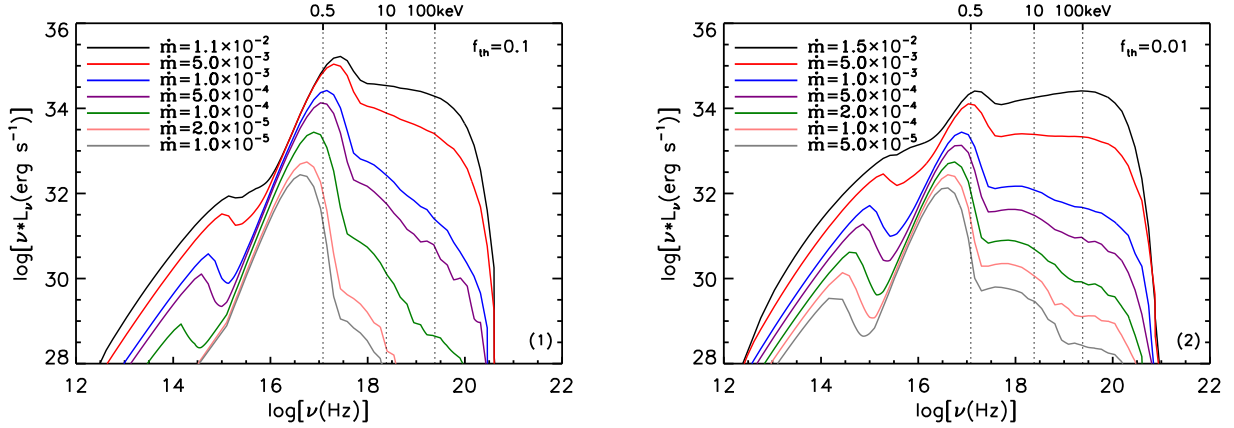


Figure 1. Panel (1): emergent spectra of NSs with an ADAF accretion for different \dot{m} with $f_{\text{th}} = 0.1$. Panel (2): emergent spectra of NSs with an ADAF accretion for different \dot{m} with $f_{\text{th}} = 0.01$.

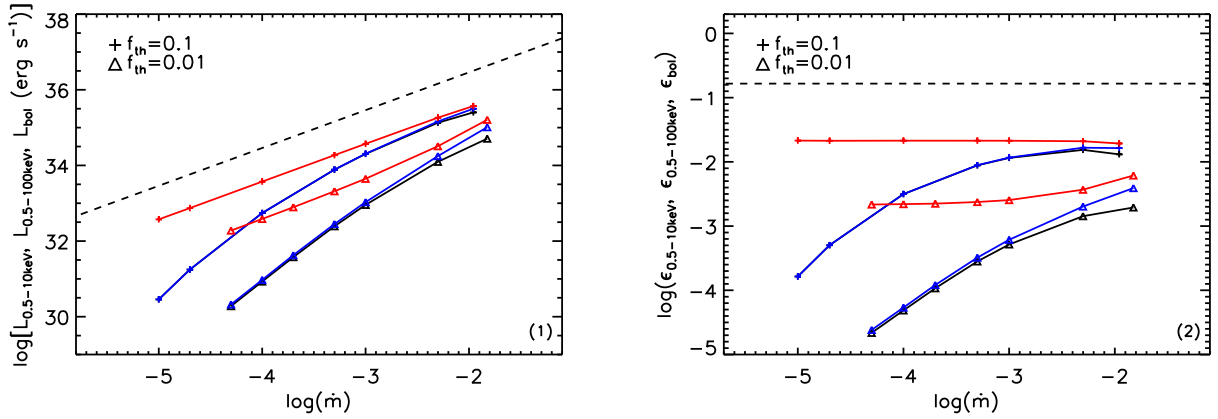


Figure 2. Panel (1): X-ray luminosity $L_{0.5-10\text{keV}}$, $L_{0.5-100\text{keV}}$ and bolometric luminosity L_{bol} as a function of \dot{m} respectively. The symbols of black '+', blue '+', and red '+' refer to $L_{0.5-10\text{keV}}$, $L_{0.5-100\text{keV}}$, and L_{bol} respectively from our model of ADAF accretion with $f_{\text{th}} = 0.1$. The symbols of black ' Δ ', blue ' Δ ', and red ' Δ ' refer to $L_{0.5-10\text{keV}}$, $L_{0.5-100\text{keV}}$, and L_{bol} respectively from our model of ADAF accretion with $f_{\text{th}} = 0.01$. The dashed line refers to the luminosity calculated with the formula of $L = \frac{MG\dot{M}}{R_*}$. Panel (2): radiative efficiency $\epsilon_{0.5-10\text{keV}}$, $\epsilon_{0.5-100\text{keV}}$ and ϵ_{bol} as a function of \dot{m} . The symbols of black '+', blue '+', and red '+' refer to $\epsilon_{0.5-10\text{keV}}$, $\epsilon_{0.5-100\text{keV}}$ and ϵ_{bol} respectively from our model of ADAF accretion with $f_{\text{th}} = 0.1$. The symbols of black ' Δ ', blue ' Δ ', and red ' Δ ' refer to $\epsilon_{0.5-10\text{keV}}$, $\epsilon_{0.5-100\text{keV}}$ and ϵ_{bol} respectively from our model of ADAF accretion with $f_{\text{th}} = 0.01$. The dashed line refers to the radiative efficiency calculated with the formula of $\epsilon = \frac{MG\dot{M}}{R_*} / \dot{M}c^2$.

Table 1. Mass accretion rate obtained for a given X-ray luminosity $L_{0.5-10\text{keV}}$ based on the curves in Fig. 3. Specifically, \dot{m}_0 and \dot{M}_0 are obtained with the formula of $\dot{M}_0 = L_{0.5-10\text{keV}} \frac{R_*}{GM} \cdot \dot{m}_0$ and \dot{M}_0 are in units of \dot{M}_{Edd} and g s^{-1} respectively. $\dot{m}_{0,1}$ and $\dot{M}_{0,1}$ are obtained from our model results of NSs with an ADAF accretion for $f_{\text{th}} = 0.1$. $\dot{m}_{0,1}$ and $\dot{M}_{0,1}$ are in units of \dot{M}_{Edd} and g s^{-1} respectively. $\dot{m}_{0,01}$ and $\dot{M}_{0,01}$ are obtained from our model results of NSs with an ADAF accretion for $f_{\text{th}} = 0.01$. $\dot{m}_{0,01}$ and $\dot{M}_{0,01}$ are in units of \dot{M}_{Edd} and g s^{-1} respectively.

$L_{0.5-10\text{keV}}$ (erg s $^{-1}$)	\dot{m}_0 (\dot{M}_{Edd})	\dot{M}_0 (g s $^{-1}$)	$\dot{m}_{0,1}$ (\dot{M}_{Edd})	$\dot{M}_{0,1}$ (g s $^{-1}$)	$\dot{m}_{0,01}$ (\dot{M}_{Edd})	$\dot{M}_{0,01}$ (g s $^{-1}$)
3.0×10^{33}	1.04×10^{-5}	2.02×10^{13}	2.82×10^{-4}	5.48×10^{14}	2.00×10^{-3}	3.88×10^{15}
5.0×10^{33}	1.73×10^{-5}	3.36×10^{13}	3.98×10^{-4}	7.75×10^{14}	3.16×10^{-3}	6.15×10^{15}

4859 and IGR J17379-3747, the results are similar to that of PSR J1023+0038. Specifically, if mass the mass accretion rate, i.e. \dot{M}_0 , is calculated with the formula of $\dot{M}_0 = L_{0.5-10\text{keV}} \frac{R_*}{GM} \cdot \dot{m}_0$, $R_{m0} > R_c$, and if the mass accretion rate, i.e. $\dot{M}_{0,1}$, is calculated with our model of ADAF accretion for $f_{\text{th}} = 0.1$, $R_{m0,1} > R_c$. In these two cases, theoretically, the pulsation cannot be formed. If the mass accretion rate, i.e. $\dot{M}_{0,01}$, is calculated with our model of ADAF accretion for

$f_{\text{th}} = 0.01$, $R_{m0,01} < R_c$. In this case, theoretically, the pulsation can be formed (Illarionov & Sunyaev 1975). One can refer to Table 2 for the detailed numerical results of R_c , R_{m0} , $R_{m0,1}$, and $R_{m0,01}$ for XSS J12270-4859 and IGR J17379-3747 respectively.

Here, we would like to remind that we take a fixed value of the NS spin frequency, i.e., $\nu_{\text{NS}} = 500$ Hz, for plotting $L_{0.5-10\text{keV}}$ as a function of \dot{m} as in Fig. 3, and the corresponding calculations for

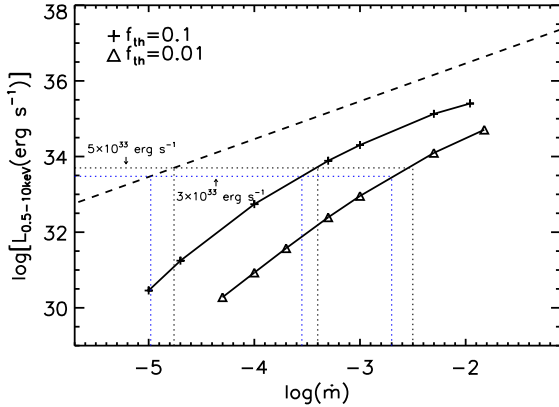


Figure 3. X-ray luminosity $L_{0.5-10\text{keV}}$ as a function of \dot{m} . The symbols of ‘+’ and ‘ Δ ’ refer to $L_{0.5-10\text{keV}}$ from our model of ADAF accretion with $f_{\text{th}} = 0.1$ and $f_{\text{th}} = 0.01$ respectively. The dashed line refers to the luminosity calculated with the formula of $L = \frac{MGM}{R_*}$. The horizontal black-dotted line refers to the X-ray luminosity of $L_{0.5-10\text{keV}} = 5 \times 10^{33} \text{ erg s}^{-1}$, and the horizontal blue-dotted line refers to the X-ray luminosity of $L_{0.5-10\text{keV}} = 3 \times 10^{33} \text{ erg s}^{-1}$. The vertical black-dotted lines from left to right refer to the value of \dot{m} of the crossing points between $L_{0.5-10\text{keV}} = 5 \times 10^{33} \text{ erg s}^{-1}$ and the formula of $L = \frac{MGM}{R_*}$, our model of ADAF accretion with $f_{\text{th}} = 0.1$, and our model of ADAF accretion with $f_{\text{th}} = 0.01$ respectively. The vertical blue-dotted lines from left to right refer to the value of \dot{m} of the crossing points between $L_{0.5-10\text{keV}} = 3 \times 10^{33} \text{ erg s}^{-1}$ and the formula of $L = \frac{MGM}{R_*}$, our model of ADAF accretion with $f_{\text{th}} = 0.1$, and our model of ADAF accretion with $f_{\text{th}} = 0.01$ respectively.

$\dot{M}_{0.1}$ (or $\dot{m}_{0.1}$) and $\dot{M}_{0.01}$ (or $\dot{m}_{0.01}$) in Table 1, which is a little different from the observed value of $\nu_{\text{NS}} = 592 \text{ Hz}$ for PSR J1023+0038, $\nu_{\text{NS}} = 593 \text{ Hz}$ for XSS J12270-4859, and $\nu_{\text{NS}} = 468 \text{ Hz}$ for IGR J17379-3747. However, we would like to remind again that it has been proven that the effect of the NS spin frequency, e.g., for taking $\nu_{\text{NS}} = 0, 200, 500$ and 700 Hz , on the structure and the emergent spectra the ADAF around a NS is very little, and nearly can be neglected (Qiao & Liu 2020a). So fixing the spin frequency at 500 Hz is a good approximation for comparing with the observational data of PSR J1023+0038, XSS J12270-4859, and IGR J17379-3747 respectively. Further, in our model of ADAF accretion, we do not consider the effect of the large-scale magnetic field, which will be discussed in Section 4.1.

Finally, we would like to mention that several other scenarios have been discussed for explaining the formation of the millisecond X-ray pulsation at the X-ray luminosity of a few times of $10^{33} \text{ erg s}^{-1}$ (e.g. Archibald et al. 2015; Papitto et al. 2015; Patruno et al. 2016; Bult et al. 2019), some of which are summarized as follows. (1) The coupling between the magnetic field lines and the highly conducting accretion flow maybe is weak, which can lead to diffusion of the gas in the accretion flow inward via Rayleigh-Taylor instability (Kulkarni & Romanova 2008), or a large-scale compression of the magnetic field (Romanova et al. 2005; Ustyugova et al. 2006; Zanni & Ferreira 2013). In these cases, even though the magnetospheric radius is greater than the corotation radius, it is possible that a fraction of the gas in the accretion flow to overcome the centrifugal barrier of the magnetic field to be accreted onto the surface of the NS forming the X-ray pulsation. (2) The interaction between the magnetosphere and the accretion disc is complex, and the ‘propeller’ effect can

reject the infalling matter in the accretion disc only if the magnetic field at the magnetospheric radius rotates significantly faster than the accretion disc (Spruit & Taam 1993). If this is not the case, instead, the magnetospheric radius of the accretion disc could be trapped near the corotation radius (Siuniae & Shakura 1977; D’Angelo & Spruit 2010, 2012), which has been used to explain the observed 1 Hz modulation in AMXP SAX J1808.4-3658 and NGC 6440 X-2 (Patruno et al. 2009; Patruno & D’Angelo 2013).

4 DISCUSSIONS

4.1 The effect of the large-scale magnetic field of $\sim 10^8 \text{ G}$ on the radiative efficiency of NSs with an ADAF accretion

In this paper, we investigate the radiative efficiency of weakly magnetized NSs with an ADAF accretion for taking two typical values of $f_{\text{th}} = 0.1$ and $f_{\text{th}} = 0.01$ as suggested in Qiao & Liu (2020a) and Qiao & Liu (2020b). Then, we show that NSs with an ADAF accretion is radiatively inefficient, with which we further explain the observed millisecond X-ray pulsations for PSR J1023+0038, XSS J12270-4859 and IGR J17379-3747 at the X-ray luminosity of a few times of $10^{33} \text{ erg s}^{-1}$. However, we should note that, in our model of NSs with an ADAF accretion, we do not consider the effect of the large-scale magnetic field on the emission of the ADAF, which probably will affect the radiative efficiency of the NSs with an ADAF accretion.

In general, accreting millisecond X-ray pulsars (AMXPs) are believed to have a relatively weaker magnetic field of $\sim 10^8 \text{ G}$ (e.g. Wijnands & van der Klis 1998; Casella et al. 2008; Patruno & Watts 2012, for review), which is different from the standard X-ray pulsars often with a stronger magnetic field of $\sim 10^{12} \text{ G}$ (e.g. Coburn et al. 2002; Pottschmidt et al. 2005; Caballero & Wilms 2012; Revnitsev & Mereghetti 2015, for review). Due to the relatively weaker magnetic field in AMXPs, it is often suggested that the magnetic field in AMXPs does not significantly affect the X-ray spectra (e.g. Poutanen & Gierliński 2003), which seems to be supported by some observations by comparing the X-ray spectra between the non-pulsating NS-LMXBs and the AMXPs. In general, it is found that there is no systematic difference of the X-ray spectra between the non-pulsating NS-LMXBs and the AMXPs in the range of $L_{0.5-10\text{keV}} \sim 10^{34} - 10^{36} \text{ erg s}^{-1}$. For example, in Wijnands et al. (2015), the author compiled a sample composed of eleven non-pulsating NS-LMXBs, finding that systematically there is an anticorrelation between the X-ray photon index Γ (obtained by fitting the X-ray spectra between 0.5 and 10 keV with a single power law) and the X-ray luminosity $L_{0.5-10\text{keV}}$ in the range of $L_{0.5-10\text{keV}} \sim 10^{34} - 10^{36} \text{ erg s}^{-1}$. Further, the authors added three AMXPs, i.e., NGC 6440 X-2, IGR J00291+5934, and IGR J18245-2452, with well measured Γ and $L_{0.5-10\text{keV}}$ to compare with the non-pulsating NS sample, showing that at a fixed X-ray luminosity, the X-ray spectra of the AMXPs appear to be slightly harder than that of the non-pulsating NS-LMXBs. More accurately, the authors did 2D KS test to study whether the AMXP data are consistent with the non-pulsating data. It is found that a 90 per cent confidence interval for the probability of $1.2 \times 10^{-6} - 3.5 \times 10^{-4}$ that the AMXP data and the non-pulsating data have the same distribution. However, given the fact that only three AMXPs are included in this study, actually, the authors also reminded that they cannot draw strong conclusions whether the presence of the magnetic field in AMXPs can alter the X-ray spectra (Wijnands et al. 2015). In a further study of Parikh et al. (2017), the authors combined the data

Table 2. The corotation radius R_c calculated with equation (4), as well as the magnetospheric radius R_{m0} , $R_{m0.1}$ and $R_{m0.01}$ calculated with equation (5), for PSR J1023+0038, XSS J12270-4859 and IGR J17379-3747 respectively. Here R_{m0} , $R_{m0.1}$ and $R_{m0.01}$ are calculated respectively by taking the mass accretion rate as \dot{M}_0 , $\dot{M}_{0.1}$, and $\dot{M}_{0.01}$ as listed in Table 1, i.e., \dot{M}_0 is obtained with the formula of $\dot{M}_0 = L_{0.5-10\text{keV}} \frac{R_c}{GM}$, $\dot{M}_{0.1}$ are obtained from our model results of NSs with an ADAF accretion for $f_{\text{th}} = 0.1$, and $\dot{M}_{0.01}$ are obtained from our model results of NSs with an ADAF accretion for $f_{\text{th}} = 0.01$. In all the calculations, we take $M = 1.4M_\odot$, $R_* = 12.5$ km, $B_* = 10^8$ G, and $\eta = 0.1$.

PSR J1023+0038 ($\nu_{\text{NS}} = 592$ Hz)				
$L_{0.5-10\text{keV}}$ (erg s $^{-1}$)	R_c (km)	R_{m0} (km)	$R_{m0.1}$ (km)	$R_{m0.01}$ (km)
3.0×10^{33}	23.8	66.2	34.2	23.1
XSS J12270-4859 ($\nu_{\text{NS}} = 593$ Hz)				
$L_{0.5-10\text{keV}}$ (erg s $^{-1}$)	R_c (km)	R_{m0} (km)	$R_{m0.1}$ (km)	$R_{m0.01}$ (km)
5.0×10^{33}	23.8	59.8	31.9	21.1
IGR J17379-3747 ($\nu_{\text{NS}} = 468$ Hz)				
$L_{0.5-10\text{keV}}$ (erg s $^{-1}$)	R_c (km)	R_{m0} (km)	$R_{m0.1}$ (km)	$R_{m0.01}$ (km)
5.0×10^{33}	27.8	62.7	33.5	22.1

in Wijnands et al. (2015) and some additional new data in the range of $L_{0.5-10\text{keV}} \sim 10^{34} - 10^{36}$ erg s $^{-1}$ for the anticorrelation between the X-ray photon index Γ and the X-ray luminosity $L_{0.5-10\text{keV}}$, the authors showed that they did not find that the X-ray spectra of AMXPs are systematically harder than that of the non-pulsating sources as tested in Wijnands et al. (2015), suggesting that the hardness of the X-ray spectra does not have strict connection with the presence of the dynamic effect of the magnetic field.

As for $L_{0.5-10\text{keV}} \lesssim 10^{34}$ erg s $^{-1}$ (generally defined as the quiescent state), the X-ray spectra of non-pulsating NS-LMXBs are very complex and diverse, which can be (1) completely dominated by a thermal soft X-ray component, (2) completely dominated by a power-law component, or (3) described by the two-component model, i.e. a thermal soft X-ray component plus a power-law component (e.g. Wijnands et al. 2015, for discussions). For example, the X-ray spectra of the non-pulsating NS-LMXB Cen X-4 at the X-ray luminosity of $L_{0.5-10\text{keV}} \sim 10^{33}$ erg s $^{-1}$ can be well fitted by the two-component model, i.e. a thermal soft X-ray component plus a power-law component, revealing a harder X-ray photon index of $\Gamma \sim 1 - 1.5$ (Chakrabarty et al. 2014; D’Angelo et al. 2015), while the X-ray spectra of several non-pulsating NS-LMXBs are well fitted by a single power law with a softer X-ray photon index of $\Gamma \sim 3 - 5$ at the X-ray luminosity of $L_{0.5-10\text{keV}} \sim$ a few times of 10^{33} erg s $^{-1}$ (Sonbas et al. 2018). For the three sources, i.e., PSR J1023+0038, XSS J12270-4859 and IGR J17379-3747 with the millisecond X-ray pulsations observed at the X-ray luminosity of $L_{0.5-10\text{keV}} \sim$ a few times of 10^{33} erg s $^{-1}$, it is found that the X-ray spectra can be well fitted by a single power law with the photon index $\Gamma \sim 1.7$ for PSR J1023+0038 (Archibald et al. 2015), with $\Gamma \sim 1.6$ for XSS J12270-4859 (Saitou et al. 2009), and can be well fitted by two thermal components, i.e., a thermal component of ~ 0.35 keV plus a thermal component of ~ 0.12 keV for IGR J17379-3747, indicating a very soft X-ray spectrum (the Group 3 data) (Bult et al. 2019).

In summary, as discussed above we think that the effect of the magnetic field of $\sim 10^8$ G in AMXPs on the emission of NSs with an ADAF accretion in the range of $L_{0.5-10\text{keV}} \sim 10^{34} - 10^{36}$ erg s $^{-1}$ is very little, consequently the effect of the magnetic field on the radiative efficiency of NSs with an ADAF accretion is very little. As for at the X-ray luminosity of $L_{0.5-10\text{keV}} \sim$ a few times of 10^{33} erg s $^{-1}$, we think it is not very easy to say whether there is significant effect of the magnetic field of $\sim 10^8$ G on the emission of NSs with an ADAF accretion. Here, at least for PSR J1023+0038 and XSS J12270-4859, if the X-ray spectra (well described by a

single power law) can be explained by our model ADAF accretion, it requires a very small value of f_{th} (for decreasing the contribution of the thermal soft X-ray component), i.e., f_{th} approaching to zero (even smaller than 0.01 as taken in the present paper) [see Fig. 7 in Qiao & Liu (2020a) for details]. So we think that our explanations for the observed millisecond X-ray pulsations at the X-ray luminosity of a few times of 10^{33} erg s $^{-1}$ with our model of ADAF accretion by taking a small value of f_{th} , i.e. $f_{\text{th}} = 0.01$ is a good approximation. Here, we would like to address that due to the existence of the magnetic field of $\sim 10^8$ G, the boundary condition in the region between the surface of the NS and the ADAF in AMXPs should be different from that of in non-pulsating NSs, which however has been incorporated into the effect of the parameter f_{th} if we only focus on this question from the viewpoint of emission. Finally, we also would like to address that a detailed study of the effects of the large-scale magnetic field of $\sim 10^8$ G on the dynamics and the emission of NSs with an ADAF accretion is still very necessary for the consistency between the model and the observations for AMXPs in the future, although the effects of the magnetic field at the strength of $\sim 10^8$ G on the radiative efficiency of NSs with an ADAF accretion maybe are not very obvious.

4.2 Further observational test for the radiative efficiency of NSs with an ADAF accretion in the future

In our model of NSs with an ADAF accretion, there is a very important parameter, f_{th} , which controls the feedback between the surface of the NS and the ADAF. The value of f_{th} can affect the radiative efficiency of NSs with an ADAF accretion. As has been shown in Qiao & Liu (2020a) and Qiao & Liu (2020b), the value of f_{th} has been constrained to be less than 0.1, and it seems that a smaller value of f_{th} , i.e., $f_{\text{th}} \sim 0.01$ is more preferred. It is possible that the remaining fraction, i.e., $1 - f_{\text{th}}$, of the ADAF energy transferred onto the surface of the NS could be partially converted to the rotational energy of the NS, and could be partially absorbed by the NS and stored as the internal energy at the crust of the NS. The accreted matter in the form of the ADAF (with relatively higher temperature and lower density) and the carried energy itself may produce some additionally observational features at the surface of the NS, which currently however has not been well investigated, depending on the resulted changes of the temperature and the density of the matter in the very thin layer at the surface of the NS (e.g. Galloway & Keek 2021, for the related discussions). The study of the further effects of the accreted matter in the form of the ADAF at the surface of the

NS exceeds the research scope in the present paper, and definitely will be carried out in the future.

In Qiao & Liu (2020a) and Qiao & Liu (2020b), the constraint to the value of f_{th} is based on some statistically observed correlations in non-pulsating NSs, such as the fractional contribution of the power-law component η as a function of $L_{0.5-10\text{keV}}$, as well as the X-ray photon index Γ as a function of $L_{0.5-10\text{keV}}$. In order more precisely to constrain the value of f_{th} , we expect that the detailed X-ray spectral fittings will be done for some typically single source in the future, such as the study for Cen X-4 (e.g. Chakrabarty et al. 2014; D’Angelo et al. 2015).

As discussed in Section 3.2, if our model of ADAF accretion can be applied to explain the observed millisecond X-ray pulsation at the X-ray luminosity of a few times of 10^{33} erg s^{-1} for PSR J1023+0038, XSS J12270-4859 and IGR J17379-3747, a small value of f_{th} , e.g., $f_{\text{th}} = 0.01$ is required. Based on some related results from the model of ADAF accretion for taking $f_{\text{th}} = 0.01$, we can further estimate the change rate of the NS spin frequency $\dot{\nu}_{\text{NS}}$. If we assume that the change of the NS spin is due to the accretion, according to the conservation of angular momentum, we have

$$I\dot{\Omega}_{\text{NS}} = \dot{M}(\Omega_* - \Omega_{\text{NS}})R_*^2, \quad (6)$$

where I is the moment of inertia of the NS, Ω_* is the rotational angular velocity of the ADAF at R_* with $\Omega_* = 2\pi\nu_*$ (with ν_* being the angular frequency at R_*), and Ω_{NS} is the rotational angular velocity of the NS with $\Omega_{\text{NS}} = 2\pi\nu_{\text{NS}}$. Rearranging equation (6), we can express the change rate of the NS spin frequency as follows,

$$\dot{\nu}_{\text{NS}} = \dot{M}(\nu_* - \nu_{\text{NS}})R_*^2/I. \quad (7)$$

Given the value of \dot{M} , ν_* , ν_{NS} and I , we can calculate the change rate of the NS spin frequency $\dot{\nu}_{\text{NS}}$. For example, for PSR J1023+0038 the millisecond X-ray pulsation is observed at the X-ray luminosity of $L_{0.5-10\text{keV}} \sim 3 \times 10^{33}$ erg s^{-1} , the corresponding \dot{M} is 3.88×10^{15} g s^{-1} based on our model of ADAF accretion for $f_{\text{th}} = 0.01$. With $\dot{M} = 3.88 \times 10^{15}$ g s^{-1} , we recalculate the structure of the ADAF for ν_* . The value of ν_* is 253 Hz. The moment of inertia I is $\sim 1.75 \times 10^{45}$ g cm^2 for taking the typical value of $M = 1.4M_{\odot}$ and $R_* = 12.5$ km respectively. The spin frequency ν_{NS} of PSR J1023+0038 is 592 Hz. Substituting the value of \dot{M} , ν_* , ν_{NS} and I into equation (7), we get $\dot{\nu}_{\text{NS}} \sim -1.2 \times 10^{-15}$ Hz s^{-1} , which is close to (~ 2.5 times less than) the observed value of $\dot{\nu}_{\text{NS}} \sim -3.04 \times 10^{-15}$ Hz s^{-1} for PSR J1023+0038 at the LMXB state (Jaodand et al. 2016). Here, we should note that in this case, the value of ν_* from our model of ADAF accretion is less than ν_{NS} , which means that a negative torque will be exerted on the NS, consequently making the rotational energy of the NS transferred onto the ADAF and the NS to be spin-down, rather than the ADAF energy transferred onto the NS and the NS to be spin-up. Further, since a variable flat-spectrum of radio emission is revealed as PSR J1023+0038 in the LMXB state, it means that the outflow is existed, which physically can further make the NS to be spin-down to match the observed $\dot{\nu}_{\text{NS}}$ (Deller et al. 2015).

A similar calculation for $\dot{\nu}_{\text{NS}}$ is done for XSS J12270-4859 and IGR J17379-3747 with the millisecond X-ray pulsations observed at the X-ray luminosity of $\sim 5 \times 10^{33}$ erg s^{-1} . At this X-ray luminosity, the mass accretion rate \dot{M} is 6.15×10^{15} g s^{-1} based on our model of ADAF accretion for $f_{\text{th}} = 0.01$. With $\dot{M} = 6.15 \times 10^{15}$ g s^{-1} , we recalculate the structure of the ADAF for ν_* . The value of ν_* is 278 Hz. The spin frequency ν_{NS} is 593 Hz for XSS J12270-4859, and is 468 Hz for IGR J17379-3747. The moment of inertia I is $\sim 1.75 \times 10^{45}$ g cm^2 for taking $M = 1.4M_{\odot}$ and $R_* = 12.5$ km

respectively. Again substituting the value of \dot{M} , ν_* , ν_{NS} and I into equation (7), we get $\dot{\nu}_{\text{NS}} \sim -1.73 \times 10^{-15}$ Hz s^{-1} for XSS J12270-4859 and $\dot{\nu}_{\text{NS}} \sim -1.0 \times 10^{-15}$ Hz s^{-1} for IGR J17379-3747. It is clear that the value of $\dot{\nu}_{\text{NS}}$ is negative (i.e., spin-down) for XSS J12270-4859 and IGR J17379-3747 as for PSR J1023+0038, which means that the rotational energy of the NS is transferred onto the ADAF. If our explanation for the formation of the observed millisecond X-ray pulsations for XSS J12270-4859 and IGR J17379-3747 at the X-ray luminosity of 5×10^{33} erg s^{-1} are correct, the predicted change rate of the NS spin frequency $\dot{\nu}_{\text{NS}}$ is at the level of $\sim -10^{-15}$ Hz s^{-1} , which we expect can be tested by the observations in the future. Further, if the change rate of the NS spin frequency $\dot{\nu}_{\text{NS}}$ predicted by our model of ADAF accretion can be confirmed in the future, which actually in turn supports our idea in the present paper that NSs with an ADAF accretion is radiatively inefficient despite the existence of the hard surface. Finally, we would like to address that the estimation of $\dot{\nu}_{\text{NS}}$ in this paper is based on our model of ADAF accretion around a weakly magnetized NS, which will make the estimated value of $\dot{\nu}_{\text{NS}}$ uncertain as applied to the AMXP cases. So the consideration of the effect of the magnetic field ($\sim 10^8$ G) on the value of $\dot{\nu}_{\text{NS}}$ in AMXPs is still very necessary in the future, which however exceeds the scope in the present paper.

5 CONCLUSIONS

Following the paper of Qiao & Liu (2020a) and Qiao & Liu (2020b) for the constraints to the value of f_{th} controlling the feedback between the surface of the NS and the ADAF, in this paper, we investigate the radiative efficiency of NSs with an ADAF accretion within the framework of the self-similar solution of the ADAF by taking two typically suggested values of f_{th} , i.e., $f_{\text{th}} = 0.1$ and $f_{\text{th}} = 0.01$ respectively. Then, we show that the radiative efficiency of NSs with an ADAF accretion is significantly lower than that of $\epsilon \sim \frac{MG\dot{M}}{R_*\dot{M}c^2} \sim 0.2$. Specifically, the radiative efficiency of our model of NSs with an ADAF accretion for $f_{\text{th}} = 0.1$ is roughly one order of magnitude lower than that of $\epsilon \sim \frac{MG\dot{M}}{R_*\dot{M}c^2} \sim 0.2$, and the radiative efficiency of our model of NSs with an ADAF accretion for $f_{\text{th}} = 0.01$ is roughly two orders of magnitude lower than that of $\epsilon \sim 0.2$. As a result, we propose that the lower radiative efficiency of our model of ADAF accretion probably can be applied to explain the observed millisecond X-ray pulsation in some NS-LMXBs (such as PSR J1023+0038, XSS J12270-4859 and IGR J17379-3747) at the X-ray luminosity (between 0.5 and 10 keV) of a few times of 10^{33} erg s^{-1} , since at this X-ray luminosity the real \dot{M} calculated with our model of ADAF accretion for taking an appropriate value of f_{th} , such as $f_{\text{th}} = 0.01$, can be more than two orders of magnitude higher than that of calculated with the formula of $\dot{M} = L_X \frac{R_*}{GM}$ to ensure a fraction of the matter in the ADAF to be channelled onto the surface of the NS forming the X-ray pulsation.

ACKNOWLEDGMENTS

Erlin Qiao thanks the very useful discussions with Dr. Chichuan Jin from NAOC. This work is supported by the National Natural Science Foundation of China (Grants 11773037 and 11673026), the gravitational wave pilot B (Grant No. XDB23040100), the Strategic Pioneer Program on Space Science, Chinese Academy of Sciences (Grant No. XDA15052100), and the National Program on Key Research and Development Project (Grant No. 2016YFA0400804).

DATA AVAILABILITY

The data underlying this article will be shared on reasonable request to the corresponding author.

REFERENCES

- Archibald A. M., et al., 2015, *ApJ*, **807**, 62
- Beri A., Altamirano D., Wijnands R., Degenaar N., Parikh A. S., Yamaoka K., 2019, *MNRAS*, **486**, 1620
- Bult P., et al., 2019, *ApJ*, **877**, 70
- Caballero I., Wilms J., 2012, *Mem. Soc. Astron. Italiana*, **83**, 230
- Casella P., Altamirano D., Patruno A., Wijnands R., van der Klis M., 2008, *ApJ*, **674**, L41
- Chakrabarty D., et al., 2014, *ApJ*, **797**, 92
- Coburn W., Heindl W. A., Rothschild R. E., Gruber D. E., Kreykenbohm I., Wilms J., Kretschmar P., Staubert R., 2002, *ApJ*, **580**, 394
- D’Angelo C. R., Spruit H. C., 2010, *MNRAS*, **406**, 1208
- D’Angelo C. R., Spruit H. C., 2012, *MNRAS*, **420**, 416
- D’Angelo C. R., Fridriksson J. K., Messenger C., Patruno A., 2015, *MNRAS*, **449**, 2803
- Degenaar N., Suleimanov V. F., 2018, *Testing the Equation of State with Electromagnetic Observations*. p. 185, doi:10.1007/978-3-319-97616-7_5
- Deller A. T., et al., 2015, *ApJ*, **809**, 13
- Done C., Gierliński M., Kubota A., 2007, *A&ARv*, **15**, 1
- Galloway D. K., Keek L., 2021, *Thermonuclear X-ray Bursts*. pp 209–262, doi:10.1007/978-3-662-62110-3_5
- Gilfanov M. R., Sunyaev R. A., 2014, *Physics Uspekhi*, **57**, 377
- Ichimaru S., 1977, *ApJ*, **214**, 840
- Illarionov A. F., Sunyaev R. A., 1975, *A&A*, **39**, 185
- Jaodand A., Archibald A. M., Hessels J. W. T., Bogdanov S., D’Angelo C. R., Patruno A. r., Bassa C., Deller A. T., 2016, *ApJ*, **830**, 122
- Kulkarni A. K., Romanova M. M., 2008, *MNRAS*, **386**, 673
- Makishima K., Maejima Y., Mitsuda K., Bradt H. V., Remillard R. A., Tuohy I. R., Hoshi R., Nakagawa M., 1986, *ApJ*, **308**, 635
- Manmoto T., Mineshige S., Kusunose M., 1997, *ApJ*, **489**, 791
- Medvedev M. V., 2004, *ApJ*, **613**, 506
- Medvedev M. V., Narayan R., 2001, *ApJ*, **554**, 1255
- Mitsuda K., et al., 1984, *PASJ*, **36**, 741
- Narayan R., Yi I., 1994, *ApJ*, **428**, L13
- Narayan R., Yi I., 1995, *ApJ*, **452**, 710
- Papitto A., de Martino D., Belloni T. M., Burgay M., Pellizzoni A., Possenti A., Torres D. F., 2015, *MNRAS*, **449**, L26
- Parikh A. S., Wijnands R., Degenaar N., Altamirano D., Patruno A., Gusinskaia N. V., Hessels J. W. T., 2017, *MNRAS*, **468**, 3979
- Patruno A., D’Angelo C., 2013, *ApJ*, **771**, 94
- Patruno A., Watts A. L., 2012, arXiv e-prints, p. arXiv:1206.2727
- Patruno A., Watts A., Klein Wolt M., Wijnand s R., van der Klis M., 2009, *ApJ*, **707**, 1296
- Patruno A., Maitra D., Curran P. A., D’Angelo C., Fridriksson J. K., Russell D. M., Middleton M., Wijnand s R., 2016, *ApJ*, **817**, 100
- Pottschmidt K., et al., 2005, *ApJ*, **634**, L97
- Poutanen J., Gierliński M., 2003, *MNRAS*, **343**, 1301
- Qiao E., Liu B. F., 2018, *MNRAS*, **481**, 938
- Qiao E., Liu B. F., 2020a, *MNRAS*, **492**, 615
- Qiao E., Liu B. F., 2020b, *MNRAS*, **496**, 2704
- Rees M. J., Begelman M. C., Blandford R. D., Phinney E. S., 1982, *Nature*, **295**, 17
- Revnivtsev M., Mereghetti S., 2015, *Space Sci. Rev.*, **191**, 293
- Romanova M. M., Ustyugova G. V., Koldoba A. V., Lovelace R. V. E., 2005, *ApJ*, **635**, L165
- Saitou K., Tsujimoto M., Ebisawa K., Ishida M., 2009, *PASJ*, **61**, L13
- Shakura N. I., Sunyaev R. A., 1973, *A&A*, **24**, 337
- Siunjaev R. A., Shakura N. I., 1977, *Pisma v Astronomicheskii Zhurnal*, **3**, 262
- Sonbas E., Dhuga K. S., Göğüş E., 2018, *ApJ*, **853**, 150
- Spruit H. C., Taam R. E., 1993, *ApJ*, **402**, 593
- Ustyugova G. V., Koldoba A. V., Romanova M. M., Lovelace R. V. E., 2006, *ApJ*, **646**, 304
- Wijnands R., van der Klis M., 1998, *Nature*, **394**, 344
- Wijnands R., Degenaar N., Armas Padilla M., Altamirano D., Cavecchi Y., Linares M., Bahramian A., Heinke C. O., 2015, *MNRAS*, **454**, 1371
- Xie F.-G., Yuan F., 2012, *MNRAS*, **427**, 1580
- Yuan F., Narayan R., 2014, *ARA&A*, **52**, 529
- Zanni C., Ferreira J., 2013, *A&A*, **550**, A99

This paper has been typeset from a $\text{\TeX}/\text{\LaTeX}$ file prepared by the author.